Available online at www.sciencedirect.com
ScienceDirect
International Journal of Heat and Mass Transfer 51 (2008) 1573–1581
International Journal of HEAT and MASS TRANSFER
www.elsevier.com/locate/ijhmt

Experimental study on the loop heat pipe with a planar bifacial wick structure

Wukchul Joung [a], Taeu Yu [b], Jinho Lee [a,*]

[a] School of Mechanical Engineering, Yonsei University, 134 Shinchon-dong, Seodaemoon-gu, Seoul 120-749, Republic of Korea
[b] Industrial Facility Team, KITECH, 35-3, Hongchon-ri, Ibjang-myun, Chonan 330-825, Republic of Korea

Received 23 February 2007; received in revised form 27 June 2007
Available online 24 October 2007

Abstract

Due to their high heat transfer efficiency, LHPs have been developing with cylindrical as well as flat evaporators for diverse applications. Nevertheless, they have limitations in applying to the closely packed heat sources such as fuel cells due to their unsuitable evaporator shape. In order to resolve this problem, a thin planar bifacial evaporator with a bifacial wick structure was devised. With the LHP developed, we examined the operating characteristics in a horizontal position for different fluid inventories. Steady state and transient state responses were studied in detail, and the relationship between fluid inventories and operational characteristics is discussed.

Keywords: Loop heat pipe; Flat evaporator; Planar bifacial wick; PEMFC thermal control; Fluid inventory

1. Introduction

Loop heat pipes (LHPs) are highly promising two-phase heat transfer devices utilizing latent heat of working fluid in transferring heat and are regarded as very efficient heat transfer devices with considerable potential for applications in various areas [1–5]. Although fundamental physical principles of the operation of LHPs are very similar to those of conventional heat pipes (HPs) and capillary pumped loops (CPLs), LHPs supplement them with new possibilities in such a way as to make it possible to manage high heat transfer capacity, create miniature or large, flexible and ramified, well-regulated and adapted designs of different shapes, and operate efficiently in any positions in a gravitational or micro-gravitational environment [6].

Since the early development of these devices, LHPs have found their applications in the thermal control of spacecraft equipment and have achieved satisfactory results [1–11]. Besides this, the development of miniature LHPs for the thermal control of highly integrated electronics is a recent trend in LHP researches [1,6,12–15]. For the applications in this area, the miniaturized LHPs with the evaporator diameter of no more than 6 mm were developed and tested. However, the development of such miniaturized LHPs has an intrinsic problem, specifically, an increased parasitic heat leak to the compensation chamber through the thin wick, which might yield the increase of the operating temperature and the minimum start-up heat load [13].

In another branch of LHP researches, there has been continuous efforts to create flat evaporator LHPs (FEL-HPs) to fit the flat thermo-contact surfaces without the use of any conventional intermediaries that cause additional thermal resistance (Fig. 1). In this way, some reported results showed that the flat evaporator LHPs, mainly of flat disc-shaped evaporator with a single evaporating surface, had operated satisfactorily and also showed possibility of a bifacial flat evaporator LHP [1,6,16–18]. However, the employment of the relatively large flat evaporator surface for such purpose may result in an intolerable internal pressure increase and higher parasitic heat leak to the compensation chamber. In particular, increased heat

* Corresponding author. Tel.: +82 2 2123 2816; fax: +82 2 312 2159.
E-mail address: jinholee@yonsei.ac.kr (J. Lee).

0017-9310/$ - see front matter © 2007 Elsevier Ltd. All rights reserved.
doi:10.1016/j.ijheatmasstransfer.2007.07.048

Nomenclature

B	coefficient
k	thermal conductivity
P	pressure
Q	heat load
r	radius of curvature of a meniscus
T	temperature

Greek symbols

ε	porosity
σ	surface tension

Subscripts

cap	capillary
eff	effective
ext	external
heat sink	heat sink
heat source	heat source
l	liquid phase
max	maximum
s	solid phase
sat	saturation
t	thermal
tot	total

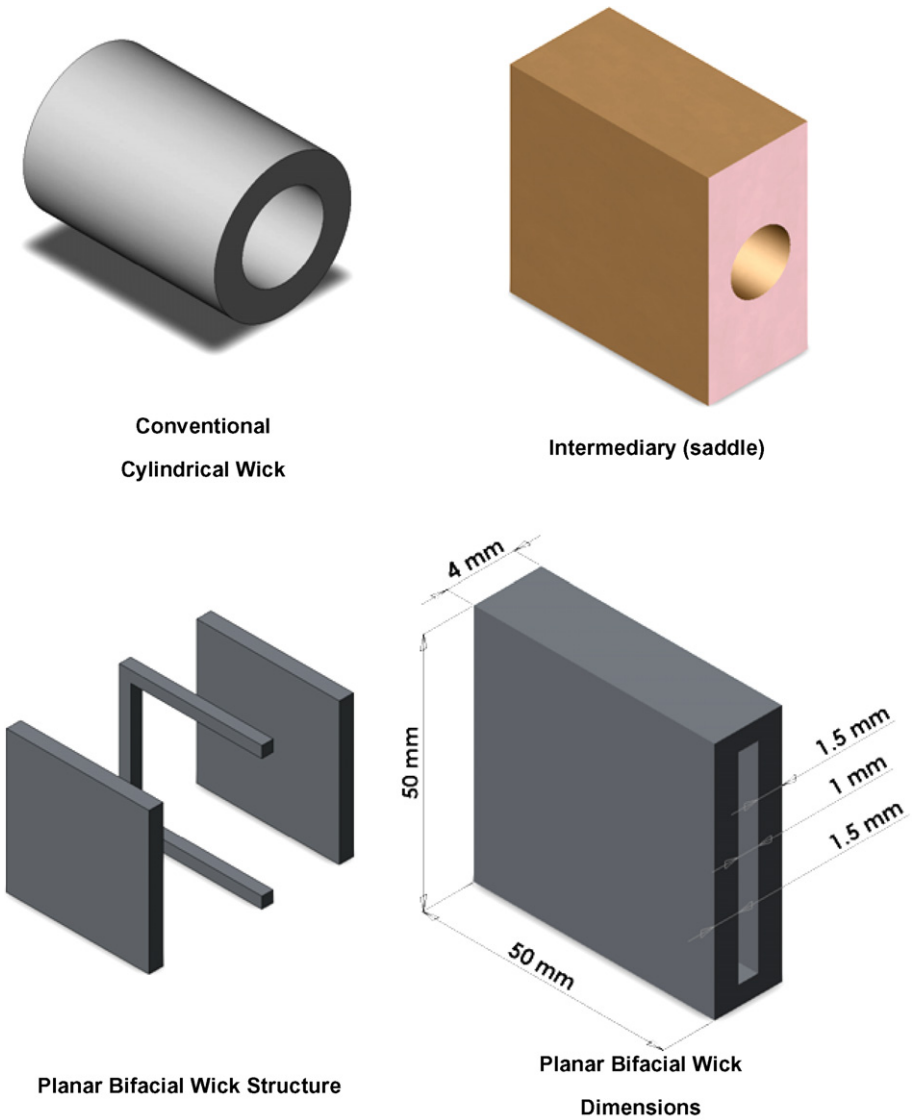

Fig. 1. Schematic of the conventional cylindrical wick structure, intermediary and the present planar bifacial wick (Stainless steel (316) porous plate of 2 μm mean pose size).

leak to the compensation chamber may result in a temperature rise of the compensation chamber, which will induce the increase of thermal resistance and start-up instability [1,6,18].

Apart from the development states of the LHPs, there have been persistent efforts to develop fuel cells with commercial feasibility to replace internal combustion engines. In this line of researches, there is an inevitable problem of operating temperature control, specifically for the PEMFC (proton exchange membrane fuel cell). The PEMFC requires the operating temperature to be less than 100 °C due to its operating conditions involving a fully water-wetted proton conductive membrane. Moreover, for acceptable operating efficiency, the working temperature should be around 80 °C. To this end, among various thermal control methods, sensible heat exchange with a coolant of large thermal mass is the most widely used method at present. However, this way of thermal control induces uneven temperature distribution along the flow path of the coolant in addition to additional power consumption. Therefore, a novel means of thermal control of the PEMFC is needed; one which not only gives even temperature distribution over an active surface of the PEMFC but also requires the least external power supply. This need motivated our present work.

The present study concerns an LHP with a thin flat evaporator incorporating bifacial (or bidirectional) heat transfer surfaces. Particularly, this work aims at the development of the flat evaporator LHP for the application to the closely packed flat heat sources such as fuel cell stacks. As an initial stage of this study, our research focused on the thermal control of PEMFCs. To this end and considering the size limitation of the fuel cells, we devised the planar bifacial wick structure fitting the flat thermo-contact surfaces of an active area of 25 cm^2, which simulate the PEMFC stack environment. We performed tests on the performance of the devised LHP for various fluid inventories, and the corresponding results are analyzed and discussed.

2. Flat bifacial evaporator loop heat pipe design and parameters

Present flat bifacial evaporator LHP (FBELHP) was devised to have flat thermo-contact surfaces and to be capable of dealing with heat loads on both sides of the evaporator. In order to create such properties, a special structure in the form of a planar bifacial wick was designed and made of sintered stainless steel (AISI 316) porous plates. The schematic of the planar bifacial wick used in this work is shown in Fig. 1. Using this wick, the evaporator with flat bidirectional thermo-contact surfaces could be realized while still retaining the structural advantages of the cylindrical wick structure.

To determine the mean pore size of the wick which determines the maximum capillary pressure on the evaporating surface of the wick, we use the first condition for LHP operation which is

$$\Delta P_{\mathrm{cap,max}} = 2\sigma/r \geqslant \Delta P_{\mathrm{tot}} \tag{1}$$

where $\Delta P_{\mathrm{cap,max}}$ is the maximum capillary pressure developed on the evaporating surface of the wick, σ is the surface tension of the working fluid, and r is the radius of curvature of a meniscus on the evaporating surface of the wick and is essentially half of the mean pore size of the wick. ΔP_{tot} is the pressure drop along the total working fluid path including filtration pressure drop. For the present planar bifacial evaporator LHP, the total pressure drop along the working fluid path at the heat load of 30 W was estimated from the manufacturer's data to be around 15 kPa for the filtration pressure drop through the wick which had the mean pore size of 2 μm and porosity of 34%. The maximum capillary pressure that could be developed on this wick is about 35 kPa at the operating temperature of 80 °C. This value was assumed to be large enough to overcome the total pressure drop along the working fluid path.

Together with the determination of the mean pore size of the wick, we estimated the thickness of the wick using the second condition of LHP operation which is given by

$$\Delta P_{\mathrm{sat}} = \left.\frac{\mathrm{d}P}{\mathrm{d}T}\right|_{\overline{T}} \Delta T_{\mathrm{sat}} = \Delta P_{\mathrm{ext}} \tag{2}$$

where ΔP_{sat} is the saturation pressure difference corresponding to the saturation temperature difference between the evaporating surface of the wick and compensation chamber. ΔP_{ext} is the pressure drop along the external flow path of the working fluid which is the same as the total pressure drop without the filtration pressure drop. We estimated the external pressure drop to be no more than 1 kPa for this system. For this amount of external pressure drop, we estimated the required saturation temperature difference at the operating temperature of 80 °C to be around 0.2 °C. In order to calculate the required thickness of the wick (at least thermodynamically), the effective thermal conductivity of the wick should be evaluated, and this can be done by using the Zehner–Schlünder correlation [19].

$$\frac{k_{\mathrm{eff}}}{k_{\mathrm{l}}} = 1 - (1-\varepsilon)^{1/2} + \frac{2(1-\varepsilon)^{1/2}}{1-\frac{k_{\mathrm{l}}}{k_{\mathrm{s}}}B}\left[\frac{\left(1-\frac{k_{\mathrm{l}}}{k_{\mathrm{s}}}\right)B}{\left(1+\frac{k_{\mathrm{l}}}{k_{\mathrm{s}}}B\right)^2}\ln\frac{1}{\frac{k_{\mathrm{l}}}{k_{\mathrm{s}}}B} - \frac{B+1}{2} - \frac{B-1}{1-\frac{k_{\mathrm{l}}}{k_{\mathrm{s}}}B}\right] \tag{3}$$

where

$$B = 1.25\left(\frac{1-\varepsilon}{\varepsilon}\right)^{10/9} \tag{4}$$

Here ε is the porosity of the wick and k_{s}, k_{l} are the thermal conductivities of the wick material and working fluid in

liquid phase, respectively. With the effective thermal conductivity, using Fourier's law of heat conduction, the required thickness of the wick was estimated at around 0.5 mm. However, the actual saturation temperature difference corresponding to the saturation pressure difference is not the saturation temperature difference across the wick, but the saturation temperature difference between the wick evaporating surface and compensation chamber. In addition, as the saturation temperature in the compensation chamber could be influenced by the possible heat leak from the evaporator, it is difficult to estimate the exact amount of heat leak across the wick. This made the calculation of the actually required wick thickness a complicated matter. Since the saturation temperature difference would be greater than the thermodynamically calculated difference, and considering the manufacturing feasibility of the desired wick structure through the sintering process, a porous plate 1.5 mm (0.6 in)-thick was selected as the wick material for this work.

For the wick fabrication, the sintered porous plate was machined to have an active area of 50 mm × 50 mm, and the resulting porous plates and porous sidewalls were welded by a laser welding machine. For the final wick structure, the planar bifacial wick had a total thickness of 4 mm including an evaporator core thickness of 1 mm (Fig. 1).

The housing (outer cover) for the evaporator and compensation chamber was made out of 1-mm thick copper and the housing wall was machined to have 12 channels on each side of its inner face for vapor removal. The channels had a depth of 0.5 mm and a width of 2 mm (Fig. 2). The compensation chamber was designed as an integral part of the evaporator, with a volume of approximately half of the total FBELHP volume. For the final product, the housing and the planar bifacial wick were welded so that the total thickness of the evaporator was 6 mm. We used a conventional copper tube (OD 3.18 mm and ID 1.76 mm) with a total length of 0.425 m for a liquid and vapor transport line and condenser. The length of vapor transport line, condenser line and liquid line were 0.16 m, 0.1 m and 0.165 m, respectively. To supply the working fluid smoothly, a bayonet made out of stainless steel pipe (OD 1.6 mm and ID 1 mm) was connected from the end of the liquid transport line to the center of the evaporator core. A schematic of the FBELHP is presented in Fig. 2.

We used methyl alcohol as the working fluid in the present study since it is less hazardous, less difficult to charge, and freezes at a lower temperature (−98 °C) than ammonia. Furthermore, methyl alcohol also gives reduced operating pressure over the whole operating range, which can considerably reduce the potential risk of high internal pressure. Regarding the compatibility of the methyl alcohol, methyl alcohol is generally known to be compatible with copper and stainless steel [20,21]. Based on component volume analysis, the minimum fluid inventory to prevent any dry-out was estimated as the charged volume of 19% of the total FBELHP volume.

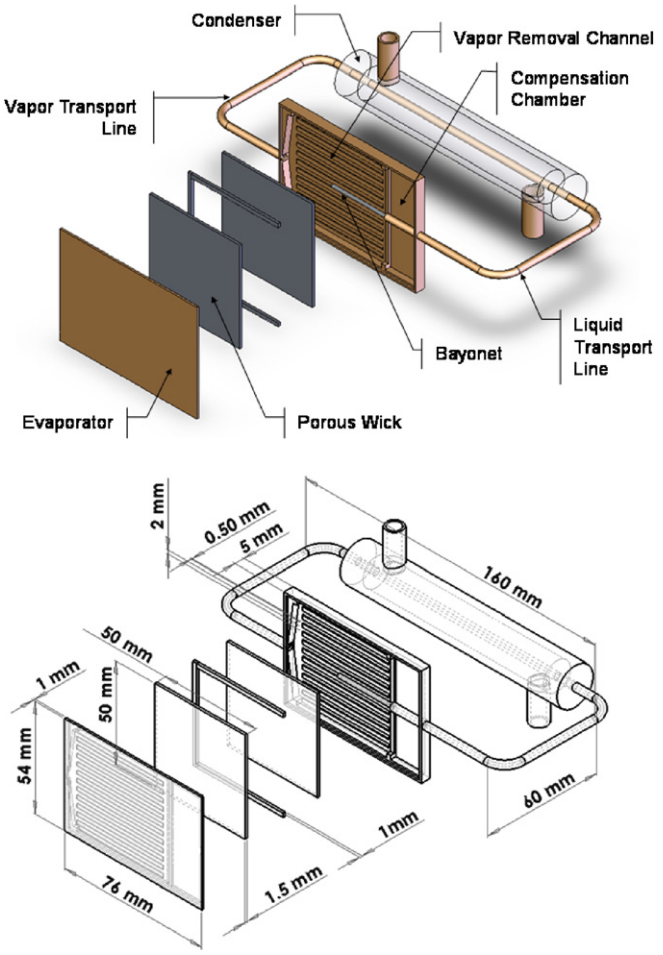

Fig. 2. Schematic of the flat bifacial evaporator loop heat pipe for the present work.

Among various parameters affecting peculiarities in the operation of LHPs, such as temperature hysteresis and temperature overshoot, the relative position of each component compared to others has been shown to have a profound effect [14]. We conducted our work in a horizontal position (zero elevation and zero tilt) where the evaporator, compensation chamber, and condenser lie in the same gravitational level, eliminating the effect of gravity.

3. Test set-up and test procedure

Fig. 3 shows the test set-up for the performance test of the FBELHP. We used a data acquisition instrument to monitor temperature readings throughout the FBELHP, where 21T-type thermocouples were embedded. The thermocouples have a deviation of ±0.3 °C at 100 °C and were connected to the Yokogawa DA-100 data acquisition instrument, which was performing readings at a frequency of 0.5 Hz. Locations of temperature readings are shown in Fig. 4. The triangles indicate measurement points on the rear side of the evaporator. The heat load was applied to the evaporator by square-type ceramic heaters (50 mm × 50 mm, 4 Ω) through copper plates of 1 mm

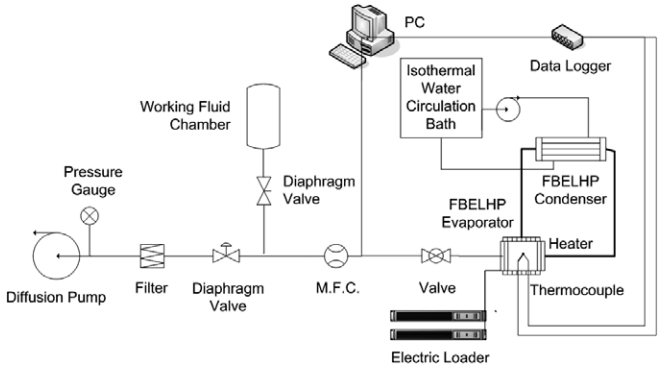

Fig. 3. Schematic of the test set-up.

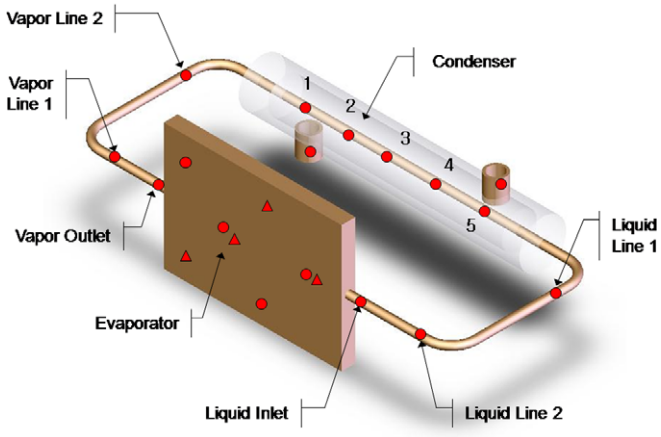

Fig. 4. Location of temperature readings.

thickness, to avoid any failure of the ceramic heaters that could be induced from possible evaporator deformation. Two identical ceramic heaters were attached to each side of the evaporator and each heater was connected to the Agilent E3648A DC power supply, which has an accuracy of ±0.2%. Heat sink (condenser) was constructed with a counter-flow heat exchanger circulating distilled water at a flow rate of 1 L/min at 25 °C. The working fluid was injected to the FBELHP through a liquid mass flow controller in an exact amount. The liquid mass flow controller used here was the BRONKHORST L1-FAC-P, which has an accuracy of less than ±1% error in the experiment range. The whole loop, including the evaporator and compensation chamber, was thermally insulated so that thermal losses or gains from the environment could be neglected.

We evaluated the performance of the FBELHP based on the operating temperature at various locations and the thermal resistance. Performance tests were carried out by measuring static responses of the FBELHP for the specified amounts of the working fluid. For each fluid inventory, the heat load was applied from the minimal value of 10 W, with 4 W increments to the maximum heat load until the operating temperature exceeded over 120 °C for safe operation. Specifically, as a thermal control means of the PEMFC, we carefully examined the operating temperatures on the heat load range of 10–30 W, corresponding to a heat dissipation range of the PEMFC with an active area of 25 cm^2. At each heat load, the FBELHP maintained operation until the steady state was reached, and measurements were made both at the transient and steady state. After the measurements were taken, the FBELHP was cooled to ambient temperature. In order to achieve a more reliable result, at least three identical tests were carried out at every heat load. Working fluid was injected to charge the FBELHP volume from 19.02% to 60.05% with an increment of 9.45% (except for 12.68% between the first and the second case). The decimals in the fluid inventories are due to the conversion factor of the mass flow controller used here. We used high-grade methyl alcohol (purity of 99.99%) as the working fluid.

4. Results and discussion

4.1. Transient state response

A representative transient state (or start-up) response of the FBELHP is presented in Fig. 5 for a fluid inventory of 60.05% and heat load of 30 W. As shown in the figure, the start-up behavior of the FBELHP is very similar to those of ordinary LHPs. At first, when the heat load was applied to the evaporator, temperatures of all components except the condenser rose together along the distance from the evaporator. At some point, due to the temperature difference between the evaporating surface of the wick and the compensation chamber, the working fluid in vapor phase began to be discharged from the evaporator, and this was made certain by the rapid increase in the temperatures of the vapor outlet, vapor line 1, and vapor line 2, in order. After some time lag, when the saturation temperature difference between the evaporating surface of the wick and the compensation chamber reached the required amount whereby the corresponding saturation pressure difference exceeded the pressure drop along the external fluid path,

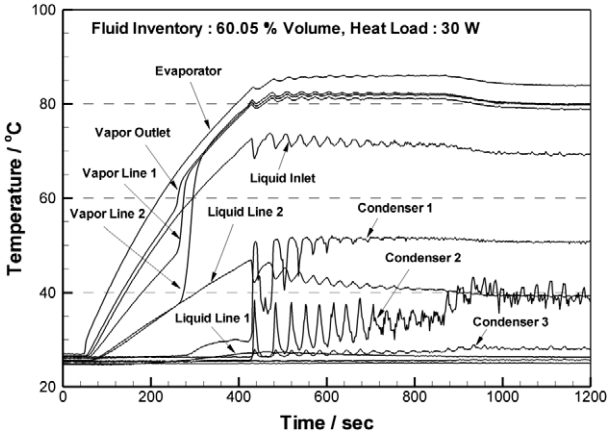

Fig. 5. Transient state response of the flat bifacial evaporator loop heat pipe.

the working fluid began to circulate throughout the entire FBELHP loop. This successful working fluid circulation was confirmed by several facts. In sequence they were as follows: the sudden increase of the condenser inlet temperature (condenser 1), fluctuating temperature at a condensation point (condenser 2 in this figure), and the gradual decrease of the temperature along the path of the subcooled working fluid in liquid phase (liquid line 1, 2, and the liquid inlet). After that, the returning cold liquid lowered the compensation chamber temperature and, in turn, the evaporator temperature. Finally, through a period of attenuation and slight overshoot, the FBELHP achieved a steady state operation.

4.2. Steady state response

Steady state performance curves of the FBELHP are presented in Figs. 6 and 7 for the operating temperature against the heat load and for the thermal resistance versus the heat load, respectively, for the specified amount of the working fluid inventories. Among the temperature readings at various locations on the evaporator, the highest value was used as the operating temperature for safety reasons. This temperature reading was consistently observed at the center of the evaporator. For the same amount of heat flux applied, the temperature readings at the front and rear side of the evaporator center were almost the same. The temperature difference between the maximum (operating) temperature and other temperatures over the evaporator surface did not exceed 2 °C. With a 95% confidence level, the operating temperatures have deviations of $T \pm 0.68$ °C, $T \pm 0.42$ °C, $T \pm 0.93$ °C, $T \pm 0.81$ °C, and $T \pm 0.7$ °C, corresponding to the operating temperature for fluid inventories of 19.02%, 31.70%, 41.15%, 50.60%, and 60.05%, respectively.

As shown in Fig. 6, the FBELHP performed very well and the results resembled performance curves of ordinary LHPs in a horizontal position. For a fluid inventory of more than 40%, the operating temperature in the heat load range of 10–30 W was well within the temperature range from 80 °C to 90 °C, which corresponds to the favorable operating temperature range of the PEMFC.

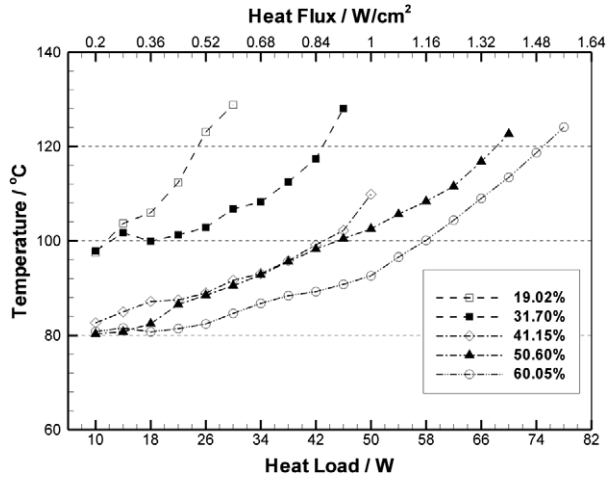

Fig. 6. Operating temperature vs. heat load for different fluid inventories.

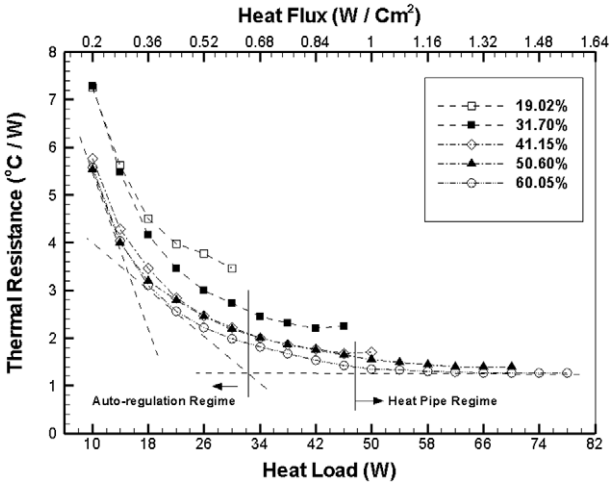

Fig. 7. Thermal resistance vs. heat load for different fluid inventories.

We observed a special characteristic of the FBELHP in a horizontal position in relation to the fluid inventory. In particular, the greater the working fluid inventory was, the lower the operating temperature was. Moreover, as the fluid inventory was increased, the operating range of the FBELHP was considerably extended. The reason for this phenomenon is explained by two facts: first, the operating temperature was closely related to the heat leak from the evaporator to the compensation chamber; and second, the planar bifacial wick and evaporator core had a rather high aspect ratio.

The operating temperature of the LHPs is generally known to be closely related to the heat leak from the evaporator to the compensation chamber [8]. The mechanism of the heat leak is conductive (when the evaporator core and wick are fully liquid-saturated) or convective (when the evaporator core and wick are partially saturated with liquid and there is any heat transfer by the working fluid in vapor phase). If the evaporator core and the wick are both fully liquid-saturated, the heat leak to the compensation chamber will be mainly by conduction through the evaporator housing and the wick, and its effect on the operating temperature will be small. However, when there is any working fluid in vapor phase in the evaporator core as is usual in the horizontal position, the heat leak increases dramatically by the simultaneous evaporation and condensation of the working fluid both in the evaporator core and in the compensation chamber (heat pipe effect). As a result, there will be a considerable increase of the LHP operating temperature. Moreover, as the heat load increases, the liquid saturation of the wick decreases and this results in an accelerated heat leak to the compensation chamber, leading to increased operating temperature. Therefore, we could easily infer that the existence of the working fluid in vapor phase in the evaporator core and the extent of

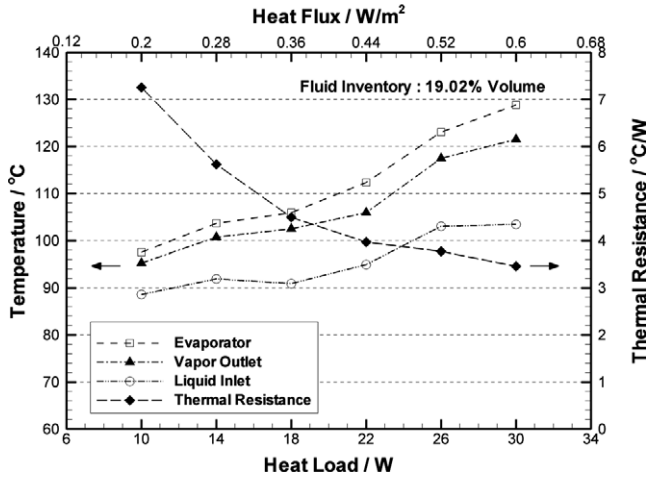

(a) Fluid inventory for 19.02% volume.

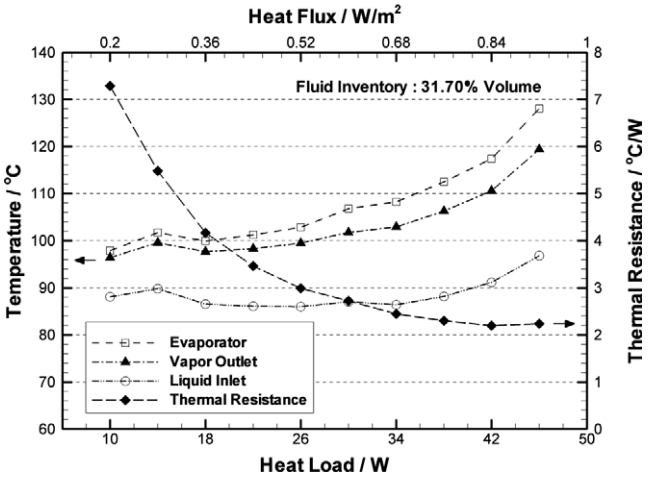

(b) Fluid inventory for 31.70% volume.

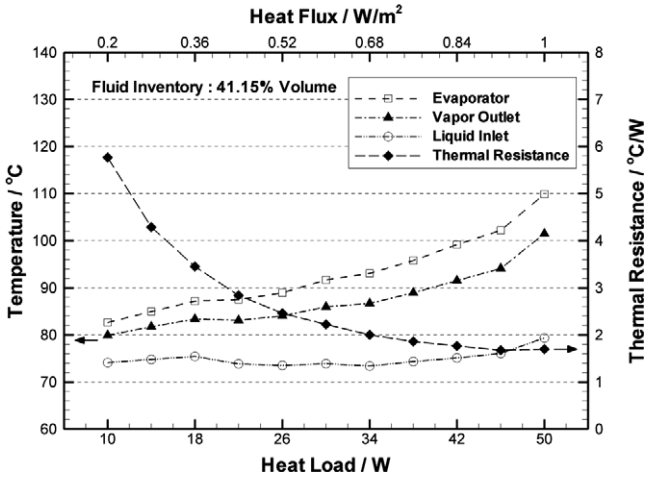

(c) Fluid inventory for 41.15% volume.

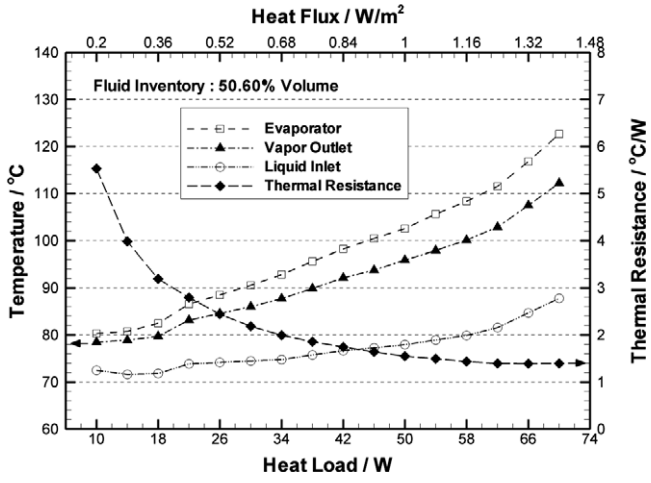

(d) Fluid inventory for 50.60% volume.

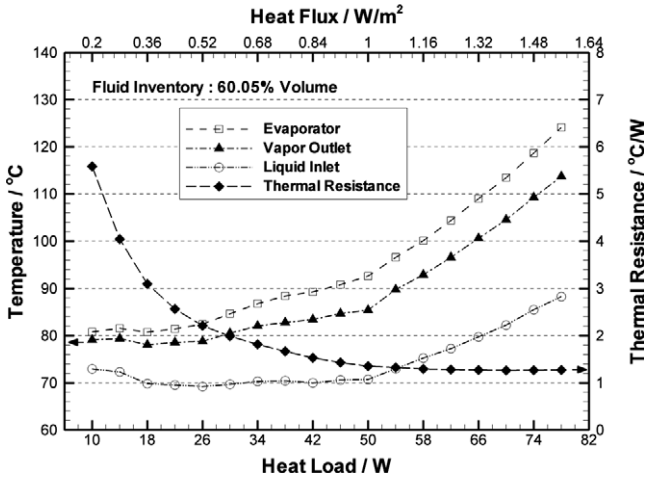

(e) Fluid inventory for 60.05% volume.

Fig. 8. Performance curves of the flat bifacial evaporator loop heat pipe for different fluid inventories.

the liquid saturation of the wick were important factors influencing the operating temperature of LHPs. As these factors are directly related to the charging of the working fluid, the fluid inventory was the key factor affecting the

operating temperature of LHPs. Note that the test set-up was placed in a horizontal position whereby the evaporator, compensation chamber, and the condenser were located at the same gravitational level, so as to have no favorable effect of gravity between components, However, since the evaporator core had a rather high aspect ratio, defined by the ratio of height to width of the evaporator core (Fig. 1), for a small amount of fluid inventory, the evaporator core was partially filled with the working fluid in liquid phase under the influence of gravity, and as a result there was working fluid in vapor phase in the evaporator core. As mentioned earlier, due to the existence of the working fluid in vapor phase, there was considerable amount of heat leak to the compensation chamber. As both the amount of the working fluid in vapor phase in the evaporator core and the amount of the heat leak to the compensation chamber are inversely related to the fluid inventory (because as the fluid inventory is increased, available space for the working fluid in vapor phase decreases and so does the amount of heat leak), the heat leak of lower fluid inventories was greater than that at higher fluid inventories. Moreover, the situation was worse as the heat load increased. As the heat load increased, hot vapor with more increased saturation pressure penetrated into a part of the wick with decreased liquid saturation and in turn accelerated the heat leak to the compensation chamber more. These features led to a higher level of the operating temperature at lower fluid inventories and a more rapid increase of the operating temperature at increasing heat loads, as shown in the performance curves of the FBELHP in Fig. 6.

The thermal resistance curves of the FBELHP (Fig. 7) show a typical trend of those of the ordinary LHPs; that is, a rapid fall followed by a gradual decrease for increasing heat load. The thermal resistance used here was the total thermal resistance defined by the ratio of temperature difference between the heat source and the heat sink to the applied heat load.

$$R_t = \frac{\Delta T}{Q} = \frac{T_{\text{heat source}} - T_{\text{heat sink}}}{Q} \tag{5}$$

The maximum value of 7.28 °C/W was obtained for the fluid inventory of 31.70% at 10 W, and the minimum value of 1.27 °C/W was obtained for the fluid inventory of 60.05% at 78 W. The thermal resistances obtained were relatively high and it was attributed to the relatively low porosity of the wick used (34%). There was not any appreciable differences in the thermal resistance for given heat loads among fluid inventories of 41.15%, 50.60%, and 60.05%, except that the range of the applied heat load depended on the fluid inventory.

For each of the fluid inventories, Fig. 8 shows the thermal resistance curves against the heat load and the temperature curves for selected locations such as the evaporator, vapor outlet, and liquid inlet. The figure shows that the FBELHP manifested both the auto-regulation regime (or variable conductance regime) and the heat-pipe regime (or constant conductance regime). The auto-regulation regime is defined as the certain range of the LHP operation in which the operating temperature decreases or remains in a certain temperature range despite the increasing heat load and is characterized by the variable thermal resistance or thermal conductance (Fig. 7). This auto-regulation regime is known to be realized by the redistribution of the working fluid between the condenser and compensation chamber. For the FBELHP, the adjusted mass flow rate of the subcooled working fluid in liquid phase to the applied heat load held the operating temperature of the FBELHP in a certain temperature range over a low heat load range and as a result the thermal resistance fell rapidly. These were assured by the temperature variations at the liquid inlet and at the vapor outlet where the temperatures more appropriately represented the working fluid temperature than the evaporator temperature and by the thermal resistance curves. As shown in Fig. 8a–c and e, the liquid inlet and vapor outlet temperatures decreased or remained nearly unchanged while the heat load kept increasing over this regime. Although there were some deviations as the heat load increased, the evaporator temperature globally confirmed this trend well, and over the auto-regulation regime, the evaporator temperature remained in a certain temperature range. Beyond this regime, a rapid increase of the operating temperature followed, and the so-called heat pipe regime began. It is characterized by constant thermal conductance or thermal resistance. The termination of the auto-regulation regime and the beginning of the heat-pipe regime can be recognized by the rapid slope change in the operating temperature curve, and it is known to begin when the condenser is fully utilized.

5. Conclusion

We designed and adopted a novel planar bifacial wick structure for the LHP with flat bifacial thermo-contact surfaces with active area of 25 cm^2. The FBELHP was tested in a horizontal position, with methyl alcohol as the working fluid for different fluid inventories. The FBELHP operated satisfactorily for a heat load range from 10 W to 78 W. The following conclusions are drawn from this study:

1. The FBELHP can start reliably with a slight overshoot (as ordinary LHPs usually do) and yield satisfactory steady state results with stable operation.
2. The FBELHP has a minimum thermal resistance of 1.27 °C/W at the maximum heat load of 78 W with a fluid inventory of 60.05%. At this maximum heat load, the operating temperature of the evaporator reached 124.1 °C.
3. The FBELHP has a lower operating temperature and more extended operating ranges at higher fluid inventories. This is attributed to the intrinsic structure of the wick and evaporator core used here, i.e. the wick and evaporator core of high aspect ratio and the extent of the liquid saturation of the wick and evaporator core.

Due to the increasing heat leak from the evaporating surface of the wick to the compensation chamber at lower fluid inventories, the FBELHP yields a higher operating temperature range than those of higher fluid inventories.

4. The FBELHP manifests the auto-regulation regime in which the operating temperature is maintained in a certain temperature range for an increasing heat load. Beyond this regime, the heat pipe regime follows a steeper slope of the operating temperature curve than that of the auto-regulation regime.
5. The FBELHP shows potential for the thermal control means of the PEMFC. It controls the operating temperature satisfactorily within the required range of the PEMFC operation.

References

[1] Yu. F. Maydanik, Loop heat pipe, Appl. Therm. Eng. 25 (2005) 635–637.
[2] J. Ku, Operating characteristics of loop heat pipes, SAE Paper No. 1999-01-2007.
[3] S. Launay et al., Parametric analysis of loop heat pipe operation: a literature review, Int. J. Therm. Sci. (2006), doi:10.1016/j.ijthermalsci.2006.11.07.
[4] T. Kaya, T.T. Hoang, Mathematical modeling of loop heat pipes and experimental validation, J. Thermophys. Heat Transfer 13 (3) (1999) 314–320.
[5] Yu. Maidanik, et al., Thermoregulation of loops with capillary pumping for space use, SAE Paper No. 921169.
[6] Yu. F. Maidanik, V.G. Pastukhov, Loop heat pipes – recent developments, test results and applications, SAE Paper No. 1999-01-2530.
[7] Yu. F. Maidanik, Y.G. Fershtater, N, Solodovnik, Loop heat pipes: design, investigation, prospects of use in aerospace techniques, SAE Paper No. 941185.
[8] Yury F. Maidanik, et al., Design and investigation of methods of regulation of loop heat pipes for terrestrial and space applications, SAE Paper No. 941407.
[9] E. Bazzo, R.R. Riehl, Operating characteristics of a small-scale capillary pumped loop, Appl. Therm. Eng. 23 (2003) 687–705.
[10] R.R. Riehl, T. Dutra, Development of an experimental loop heat pipe for application in future space missions, Appl. Therm. Eng. 25 (2005) 101–112.
[11] Roger R. Riehl, Tulio C.P.A. Siquera, Heat transport capability and compensation chamber influence in loop heat pipes performance, Appl. Therm. Eng. 26 (2006) 1158–1168.
[12] V.G. Pastukhov et al., Miniature loop heat pipes for electronics cooling, Appl. Therm. Eng. 23 (2003) 1125–1135.
[13] Yury F. Maydanik, Sergey V. Vershinin, Mikhail A. Korukov, Miniature loop heat pipes – a promising means for cooling electronics, in: Proceedings of the 9th International Society Conference on Thermal and Thermomechanical Phenomena in Electronic Systems, Las Vegas, NV, 2004, pp. 60–66.
[14] Yuming Chen et al., Steady-state and transient performance of a miniature loop heat pipe, Int. J. Therm. Sci. 45 (2006) 1084–1090.
[15] V.G. Pastukhov, Y.F. Maydanik, Low-noise cooling system for PC on the base of loop heat pipes, Appl. Therm. Eng. 27 (2007) 894–901.
[16] Yu. F. Gerasimov, et al., USSR Inventor's Certificate #495522, 1975.
[17] Yu. F. Maidanik, S.V. Vershinin, Patent of Russia #2101644, 1998.
[18] Yu. F. Maidanik, et al., Development and tests of miniature loop heat pipe with a flat evaporator, SAE Paper No. 2000-01-2491.
[19] M. Kaviany, Principles of Heat Transfer in Porous Media, second ed., Springer-Verlag, New York, 1995, pp. 144–147.
[20] P.D. Dunn, D.A. Reay, Heat Pipes, fourth ed., Pergamon, 1994, pp. 126–138.
[21] Amir Faghri, Heat Pipe Science and Technology, Taylor & Francis, New York, 1995, pp. 19–24.